ISBN: 978-3-95450-236-3 ISSN: 2673-5350 doi:10.18429/JACoW-IBIC2023-MO2I02

FAST ORBIT FEEDBACK FOR DIAMOND-II

I. Kempf *, M. Abbott, L. Bobb, G. B. Christian, Diamond Light Source, Oxfordshire, UK
G. Rehm, Helmholtz-Zentrum für Materialien und Energie, Berlin, Germany
S. Duncan, University of Oxford, Oxford, UK

Abstract

The electron beam stability is critical for 4th generation light sources. As opposed to 10 % of beam size up to 140 Hz at Diamond, advances in detector speed and resolution at Diamond-II increase the stability requirements to 3 % up to 1 kHz. This paper presents a novel control methodology for the fast orbit feedback at Diamond-II, which will stabilise the beam using two arrays of 252 slow and 144 fast correctors and 252 beam position monitors at 100 kHz. In contrast to existing approaches that separate slow and fast feedback loops, our approach is based on a two-matrix factorisation called the generalised singular value decomposition (GSVD), which decouples the system into 144 two-input modes controlled by slow and fast magnets and 108 modes controlled by slow magnets only. The GSVD-based controller is implemented in the existing Diamond storage ring using a centralised communication architecture, such as planned for Diamond-II. We present results from the Diamond storage ring and simulation, which confirm that the proposed approach meets the target specification for Diamond-II.

INTRODUCTION

The fast orbit feedback (FOFB) at Diamond Light Source (Diamond) attenuates disturbances of the electron beam in the storage ring. Disturbance sources include ground and girder vibrations, power supply and RF noise, and transients induced by insertion device (ID) gap changes. At Diamond, the FOFB uses 173 electron beam position monitors (BPMs) measuring both horizontal and vertical positions, and 172 vertical and 172 horizontal correctors to perform global orbit correction of the electron beam at 10 kHz. The FOFB reduces the root-mean square (RMS) deviation of the electron beam to within 10 % of the beam size up to a closed-loop bandwidth of 140 Hz, i.e. the frequency at which disturbances are attenuated by 3 dB. For Diamond-II, advances in beamline technology require the closed-loop bandwidth to be increased to 1 kHz, while the new multi-bend achromat lattice will reduce the beam size [1], resulting in the increased beam stability requirements summarised in Table 1 (top).

To meet these requirements, the FOFB hardware and software for Diamond-II have been redesigned, increasing the specifications as shown in Table 1 (bottom). Firstly, the sampling frequency is increased to 100 kHz and the overall latency reduced to 100 µs. Secondly, the number of BPMs is increased to 252. Finally, to achieve the 1 kHz closed-loop bandwidth, the open-loop bandwidth, i.e. the overall corrector bandwidth, is increased from 500 Hz to ≥ 5 kHz by introducing two types of correctors: 252 slow correctors producing a deflection of 1 mrad, and 144 fast correctors producing a deflection of 20 µrad [1].

Table 1: Top: Beam size, relative and absolute orbit stability requirements at standard straight source points. Bottom: FOFB specifications. Tables adapted from Ref. [1].

Parameter	Diamond	Diamond-II
Beam size H/V	123 µm/3.5 µm	30 µm/4 µm
Rel. stability	10 % up to 100 Hz	3 % up to 1 kHz
Abs. stability H/V	12 µm/0.35 µm	0.9 µm/0.12 µm
Closed-loop BW	140 Hz	≥ 1 kHz
Latency	700 µs	≤ 100 µs
BPMs	173	252
Correctors	172	252 slow/144 fast

H: horizontal, V: vertical, BW: bandwidth

While using two types of correctors allows the closed-loop bandwidth to be increased, it prohibits the existing FOFB control algorithm to be reused, which is based on diagonalising the dynamics using the modal decomposition and controlling the single-input single-output (SISO) modal dynamics. Although extensions of modal decomposition have been proposed in [2, 3], they leave the decoupling process unspecified for systems with fewer fast than slow correctors. For Diamond-II, we propose a joint design method based on the generalised singular value decomposition (GSVD) [4] to decouple the system into sets of two-input single-output (TISO) and SISO systems. It can be shown that the generalised modal decomposition of a system with two corrector types is closely related to the modal decomposition of a system with one corrector type, which allows techniques to be carried over to the system with two corrector types, including regularisation gains that account for a large condition number of the orbit response matrix (ORM).

Based on the assumption that the bandwidths of the slow and fast correctors differ significantly, other approaches split the control problem into two separate feedback loops: one feedback loop for the slow correctors that may be operated at a lower sampling/actuation frequency, and a separate feedback loop for the fast correctors. Such a separation is implemented in most synchrotrons that use separate sets of slow and fast correctors [5–7], but interactions at intermediate frequencies can require the introduction of a frequency deadband between the slow and fast loops [8]. Depending on the disturbance spectrum, this approach can lead to significant performance degradation [6]. One common way

* Corresponding author: idris.kempf@eng.ox.ac.uk. Also at University of Oxford. This work was supported in part by Diamond Light Source and in part by the Engineering and Physical Sciences Research Council (EPSRC) with a Collaborative Awards in Science and Engineering (CASE) studentship.

ISBN: 978-3-95450-236-3 ISSN: 2673-5350 doi:10.18429/JACoW-IBIC2023-MO2I02

to avoid introducing a frequency deadband is to subtract the predicted effect of the slow correctors from the feedback signal for the fast correctors [5]. Another solution is to periodically subtract the DC gain from each fast corrector (individually) and to import these values into the slow feedback loop, thereby shifting the low-frequency action from the fast correctors to the slow correctors [9]. However, this approach neglects the coupling between slow and fast correctors and relies on a SISO analysis of the combined slow and fast loops. As in the case of systems with one corrector type, large condition numbers of the ORM limit the closed-loop bandwidth [10], and neglecting the coupling may require further reduction of controller gains [11]. None of these approaches – the frequency deadband method [5], the periodic DC method [9], or combinations of those [11, 12] – provide a means of jointly investigating the stability, performance and robustness properties of the combined feedback loops.

This paper presents the controller design for Diamond-II using preliminary corrector models, and summarises the GSVD-based controller [13]. To estimate the FOFB performance at Diamond-II, predictions of the Diamond-II disturbance [14] are used for obtaining worst-case estimates of the beam displacement. To validate these theoretical expectations, the algorithm is implemented and tested on the existing Diamond storage ring.

DIAMOND-II CONTROLLER DESIGN

Background: The Existing System

The electron beam dynamics at Diamond are modelled by a cross-directional system with one corrector type [10]:

$$y(s) = Rg(s)u(s) + d(s), \tag{1}$$

where $R \in \mathbb{R}^{n_y \times n_u}$ is the ORM, $s \in \mathbb{C}$ the Laplace variable, $u(s) \in \mathbb{C}^{n_u}$ are the corrector currents (inputs), $y(s) \in \mathbb{C}^{n_y}$ the BPM signals (outputs) and $d(s) \in \mathbb{C}^{n_y}$ the disturbances. The coupling between the planes is negligible so the horizontal and vertical orbit corrections are treated as separate control problems. The stable transfer function $g(s) \in \mathbb{C}$ captures the temporal dynamics of the correctors and is modelled as $g(s) := a/(s+a)\mathrm{e}^{-\tau_d s}$, where $a := 2\pi \times 700\,\mathrm{rad\,s^{-1}}$ is the magnet bandwidth and $\tau_d := 900\,\mu\mathrm{s}$ the time delay [10]. At Diamond, the controller is designed in modal space, i.e. the thin singular value decomposition (SVD) $R = U\Sigma V^{\mathrm{T}}$ is substituted in Eq. (1) and decoupled as $\hat{y}(s) = \Sigma g(s)\hat{u}(s) + \hat{d}(s)$, where $\hat{y}(s) := U^{\mathrm{T}}y(s)$, $\hat{u}(s) := V^{\mathrm{T}}u(s)$, $\hat{d}(s) := U^{\mathrm{T}}d(s)$. In modal space, the multi-input multi-output (MIMO) control problem is simplified to n_y decoupled SISO problems.

The Diamond-II System

For Diamond-II, the beam will be monitored by $n_y = 252$ BPMs, with primary BPMs located upstream and downstream of each ID. The front-end X-ray BPMs are integrated into the 100 kHz data stream so that primary (electron) BPMs can be substituted for front-end X-ray BPMs by providing the corresponding ORM, increasing the fault tolerance and allowing source point control of bending magnet beamlines. The FOFB will use $n_s = 252$ slow correctors with a bandwidth of ~ 200 Hz and $n_f = 144$ fast correctors with a bandwidth of ~ 8 kHz. The electron beam dynamics for the system with two corrector types are

$$y(s) = R_s g_s(s)u_s(s) + R_f g_f(s)u_f(s) + d(s), \tag{2}$$

where $R_s \in \mathbb{R}^{n_y \times n_s}$, $R_f \in \mathbb{R}^{n_y \times n_f}$, $n_y = n_s = 252$ and $n_f = 144$. The preliminary corrector models $g_s(s)$ and $g_f(s)$ include the frequency responses of the DAC, ADC, signal processing filters, power supplies, magnets, and copper vessel for slow correctors and stainless steel vessel for fast correctors, resulting in 2nd- and 3rd-order transfer functions. Note that since $n_s = n_y$, the FOFB can also be operated using slow correctors only, or fast correctors substituted for slow ones.

To reduce the latency in the FOFB loop, the FOFB communication network will be changed from a distributed topology to a centralised topology [1], and the centralised controller is planned to be implemented on the FPGA of a White Rabbit switch v4 (WRSv4). The time delay of $g_{(\cdot)}(s)$ is assumed to be 100 µs, which is a worst-case upper bound of the latency estimates for Diamond-II. The latency estimate includes 39.35 µs for signal processing (DAC, ADC, BPM), 8 µs for communication, 20 µs for FOFB computations, and 30 µs to account for uncertainty in the fast corrector model.

Decoupling the Diamond-II System

Analogous to the SVD for systems with one corrector type, the GSVD [4] factorises R_s and R_f as

$$R_s = X\begin{bmatrix}\Sigma_s & 0\\ 0 & I\end{bmatrix}U_s^{\mathrm{T}}, \qquad R_f = X\begin{bmatrix}\Sigma_f\\ 0\end{bmatrix}U_f^{\mathrm{T}}, \tag{3}$$

where $X = [x_1 \ldots x_{n_y}] \in \mathbb{R}^{n_y \times n_y}$ with $\det(X) \neq 0$, is the shared matrix of generalised output modes, $\Sigma_{(\cdot)} = \mathrm{diag}(\sigma_{(\cdot),1}, \ldots, \sigma_{(\cdot),n_f}) > 0$ with $(\cdot) = \{\mathrm{s}, \mathrm{f}\}$ are the matrices of generalised singular values that satisfy $\sigma_{\mathrm{s},i}^2 + \sigma_{\mathrm{f},i}^2 = 1$, and $U_{(\cdot)} \in \mathbb{R}^{n_{(\cdot)} \times n_{(\cdot)}}$ with $U_{(\cdot)}^{\mathrm{T}}U_{(\cdot)} = I$ are the matrices of generalised input modes. In contrast to the standard singular values that measure the gain in the direction of the singular vectors, the generalised singular values measure the relative gain of slow and fast correctors in the direction of x_i. It can be shown that the matrices X and $R = [R_s\ R_f]$ share the same standard singular values and left singular vectors [13], relating the modal decomposition to the generalised modal decomposition. For Diamond-II, the condition numbers are $\kappa(X) = 4404$ for the vertical and $\kappa(X) = 2371$ for the horizontal planes, and the generalised singular values satisfy $1 < \kappa(\Sigma_s) < 2$ and $1 < \kappa(\Sigma_f) < 2$.

Substituting the GSVD in Eq. (2) and left-multiplying with X^{-1} decouples the system with two corrector types as

$$\tilde{y}(s) = \begin{bmatrix}\Sigma_s & 0\\ 0 & I\end{bmatrix}g_s(s)\tilde{u}_s(s) + \begin{bmatrix}\Sigma_f\\ 0\end{bmatrix}g_f(s)\tilde{u}_f(s) + d(s), \tag{4}$$

where $\tilde{y}(s) := X^{-1}y(s)$, $\tilde{u}_{(\cdot)}(s) := U_{(\cdot)}^{\mathrm{T}}u_{(\cdot)}(s)$ and $\tilde{d}(s) := X^{-1}d(s)$. The decoupled systems shows that for $n_f < n_s =$

ISBN: 978-3-95450-236-3 ISSN: 2673-5350 doi:10.18429/JACoW-IBIC2023-M02I02

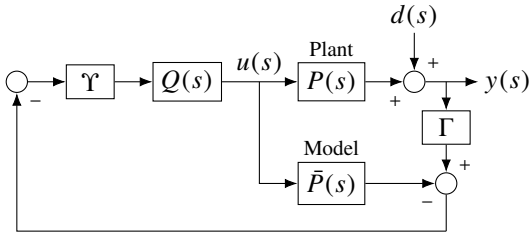

Figure 1: IMC structure in original space with additional compensators Υ and Γ.

n_y, only a subset of the disturbances is attenuated by slow and fast correctors, i.e. those lying entirely in $\text{span}(x_1, \ldots, x_{n_f})$.

TISO and SISO Controllers

Equation (4) reads row-wise as $\tilde{y}_i(s) = \tilde{P}_i(s)\tilde{u}_i(s) + \tilde{d}_i(s)$, where for $i \in \mathcal{I}_{\text{tiso}} := \{1, \ldots, n_f\}$, $\tilde{P}_i(s) := [\sigma_{s,i} g_s(s), \sigma_{f,i} g_f(s)]$, $\tilde{Q}_i(s) := [q_{s,i}(s), q_{f,i}(s)]^T$, and $\tilde{u}_i(s) := [u_{s,i}(s), u_{f,i}(s)]^T$, and for $i \in \mathcal{I}_{\text{siso}} := \{n_f + 1, \ldots, n_s\}$, $\tilde{P}_i(s) := g_s(s)$, $\tilde{Q}_i(s) := q_{s,i}(s)$, and $\tilde{u}_i(s) := \tilde{u}_{s,i}(s)$. Although any control approach including PID control could be applied, the internal model control (IMC) structure is used [15], which is naturally amenable to time delays and also used at Diamond. The IMC structure is shown in is shown in Fig. 1 in original space, where Υ and Γ are matrices that will be considered in the following section. For the remainder of this paper, the plant model is assumed to be accurate, i.e. $P_i(s) = \bar{P}_i(s)$ and $\tilde{P}_i(s) = \tilde{\bar{P}}_i(s)$, so that the control inputs are $\tilde{u}_i(s) = -\tilde{Q}_i(s)\tilde{d}_i(s)$. Substituting in the row-wise dynamics yields $\tilde{y}_i(s) = \big(1 - \tilde{P}_i(s)\tilde{Q}_i(s)\big)\tilde{d}_i(s)$. First, the desirable closed-loop dynamics are defined as

$$\tilde{y}_i(s) = \big(1 - T_{(\cdot)}(s)\big)\tilde{d}_i(s) \quad \text{for } i \in \mathcal{I}_{(\cdot)}, \tag{5}$$

for $(\cdot) = \{\text{tiso}, \text{siso}\}$ and where the complementary sensitivities must satisfy $T_{(\cdot)}(0) = 1$ for a zero steady-state error. Secondly, the controller structure is simplified as $\tilde{k}_{(\cdot),i} \times f_{(\cdot)}(s)$ for $(\cdot) = \{\text{s}, \text{f}\}$, so that equating Eq. (5) and the row-wise dynamics yields

$$q_{(\cdot)}(s) := \tilde{k}_{(\cdot),i} T_{(\cdot)}(s) / g_{(\cdot)}(s), \tag{6}$$

for $(\cdot) = \{\text{s}, \text{f}\}$ and where $T_s(s) := T_{\text{siso}}(s)$ and $T_f(s) := T_{\text{tiso}}(s) - T_{\text{siso}}(s)$, and $\tilde{k}_{s,i} := 1/\sigma_{s,i}$ and $\tilde{k}_{f,i} := 1/\sigma_{f,i}$ for $i \in \mathcal{I}_{\text{tiso}}$, and $\tilde{k}_{s,i} = 1$ for $i \in \mathcal{I}_{\text{siso}}$. The controller in Eq. (6) splits the control effort between slow and fast correctors and is also referred to as mid-ranging controller [16].

For Diamond-II, the corrector models $g_s(s)$ and $g_s(s)$ are 2nd- and 3rd-order transfer functions with a time delay of $\tau_d = 100\,\mu\text{s}$, so the complementary sensitivities are chosen as $T_{(\cdot)}(s) := \omega_{(\cdot)}/(s + \omega_{(\cdot)}) \times H_{2,(\cdot)}(s)e^{-s\tau_d}$, where $(\cdot) = \{\text{tiso}, \text{siso}\}$ and $H_{2,(\cdot)}(s)$ is a second-order Butterworth filter [15] with a cutoff frequency of 500 Hz for SISO and 10 kHz for TISO systems.

Tuning for Expected Disturbances

The controller is tuned based on the estimated power spectral density (PSD) of the disturbance for Diamond-II, which

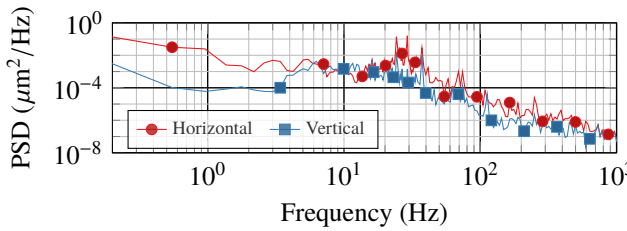

Figure 2: Estimated power spectral density (PSD) of the uncorrected vertical disturbance for Diamond-II at the upstream primary BPM on the first standard straight [14].

is shown in Fig. 2 for the upstream primary BPM on the first standard straight [14]. The PSD includes contributions from ground vibrations, girder motion, power supply ripple and RF noise.

The closed-loop bandwidth of the slow correctors, ω_{siso}, is limited by rate constraints of the power supplies, but must be chosen high enough to deliver low-frequency disturbance attenuation across all n_y directions. According to Fig. 2, the PSD drops by several orders of magnitude above 100 Hz, so ω_{siso} is chosen as $\omega_{\text{siso}} = 2\pi \times 100\,\text{rad}\,\text{s}^{-1}$. Note that if ω_{siso} is chosen larger than the open-loop bandwidth of $g_s(s)$, the controller will result in large corrector gains above the open-loop bandwidth.

Although a large ω_{tiso} yields a large overall closed-loop bandwidth, in the presence of large time delays it can cause disturbances to be amplified by a large sensitivity peak, i.e. large values of $S_{\max} := \max_\omega |S_{\text{tiso}}(\text{j}\omega)|$. Moreover, large ω_{tiso} may cause disturbances at high frequencies (i.e. above the closed-loop bandwidth) to be amplified, and make the controller prone to instabilities [15]. A bandwidth of 1 kHz for $S_{\text{tiso}}(s)$ results in $S_{\max} = 6\,\text{dB}$ at 5 kHz, so the bandwidth is reduced to 600 Hz ($\omega_{\text{tiso}} = 2\pi \times 2\,\text{krad}\,\text{s}^{-1}$), giving $S_{\max} = 4.12\,\text{dB}$ at 2.2 kHz. Note that with a time delay of 70 µs instead of 100 µs, the peak could be reduced to 2.4 dB, or the closed-loop TISO bandwidth increased to 1 kHz with $S_{\max} = 4.12\,\text{dB}$.

Structure in Original Space

After designing the TISO and SISO controllers for the decoupled systems, the modal controllers in Eq. (6) are concatenated and mapped back to original space to obtain the control inputs as $u_{(\cdot)}(s) = -Q_{(\cdot)}(s)d(s)$ with $Q_{(\cdot)}(s) := K_{(\cdot)}q_{(\cdot)}(s)$ and $K_{(\cdot)} := U_{(\cdot)}\tilde{K}_{(\cdot)}X^{-1}$. Substituting the control inputs in Eq. (2) yields the closed-loop dynamics in original space:

$$y(s) = \Big(I - IT_{\text{siso}}(s) - X_{\text{tiso}}X^{-1}T_f(s)\Big)d(s), \tag{7}$$

where $X_{\text{tiso}} := \big[x_1, \ldots, x_{n_f}, 0, \ldots, 0\big]$. Since $\kappa(X) = \kappa(R) \gg 1$, the inverse X^{-1} in $K_{(\cdot)}$ produces large controller gains in directions associated with the small singular values of R. Moreover, the term associated with the $n_f < n_s$ fast correctors in Eq. (7) amplifies certain disturbance directions when X is not orthogonal.

ISBN: 978-3-95450-236-3 ISSN: 2673-5350 doi:10.18429/JACoW-IBIC2023-MO2I02

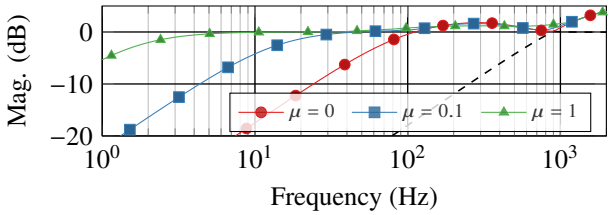

(a) MIMO sensitivity.

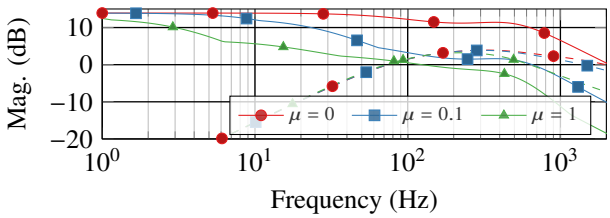

(b) MIMO controller gains.

Figure 3: Minimum (dashed) and maximum singular values of the sensitivity $S(\mathrm{j}\omega)$ for different values of μ (a), and controller gains for slow and fast (dashed) correctors (b).

In original space, two compensators, $\Upsilon \in \mathbb{R}^{2n_y \times n_y}$ and $\Gamma \in \mathbb{R}^{n_y \times n_y}$, are added to the IMC structure in Fig. 1, where $P(s) := [R_s g_s(s)\ R_f g_f(s)]$, $Q(s) := \mathrm{diag}(Q_s(s), Q_f(s))$, and $u(s) := [u_s(s)^T\ u_f(s)^T]^T$. The compensator $\Upsilon := [I\ \Upsilon_f^T]^T$ with $XX^{\dagger}_{\mathrm{tiso}}$ only applies to the case $n_f < n_s$ and projects $d(s)$ onto $x_1, \ldots, x_{n_f}$ for the TISO systems [13].

The compensator Γ reduces the controller gain and is defined as $\Gamma := (XX^T + \mu I)^{-1} XX^T$, where $\mu \in \mathbb{R}_{\geq 0}$ is a regularisation parameter [13]. With Υ and Γ, the closed-loop dynamics are $y(s) = S(s)d(s)$, where the sensitivity $S(s)$ is

$$S(s) := I - P(s)Q(s)\Upsilon(I + (\Gamma - I)P(s)Q(s)\Upsilon)^{-1}\Gamma. \quad (8)$$

The effect of Γ on the minimum and maximum singular values of $S(\mathrm{j}\omega)$ is shown in Fig. 3a for $\mu = \{0, 0.1, 1\}$. The maximum singular values of the transfer functions from $d(s)$ to $u_s(s)$ and $u_f(s)$ are shown in Fig. 3b. As μ increases, the overall bandwidth decreases, but the minimum singular values (dashed) remain unchanged. It can be shown that the bandwidth is reduced for higher modes of $R = [R_s\ R_f]$ that satisfy $\sigma_i^2 \ll \mu$. As most of the disturbances are input disturbances, most of the disturbances occur within the lower order modes, which justifies the use of the compensator Γ [13]. For Diamond-II, μ is chosen as $\mu = 0.1$, yielding a fast corrector demand of 276 mA and 92 mA in the horizontal and vertical direction up to 1 kHz, which is below the maximum demand of 920 mA.

Expected Performance

Although the PSDs from Fig. 2 can be used to design the TISO and SISO controllers, they lack the phase information that is required to describe the spatial distribution across the storage ring needed for the MIMO analysis. However, an upper bound on the amplitude spectral density (ASD) $|Y_i(\omega_k)|$ – the square root of the PSD – at BPM i can be obtained from

$$|Y_i(\omega_k)| \leq \sum_{j=1}^{n_y} |S_{ij}(\omega_k)||D_j(\omega_k)|, \quad (9)$$

where $S_{ij}(\omega_k)$ refers to row i and column j of $S(\cdot)$ in Eq. (8) and $D_j(\omega_k)$ to the disturbance at BPM j. Another upper bound is $|Y_i(\omega_k)| \leq \|Y(\omega_k)\|_2 \leq \|S(\omega_k)\|_2 \|D(\omega_k)\|_2$, though this is always equally or more conservative than the bound in Eq. (9).

In addition, the performance can be estimated with simulations that use disturbances obtained from sampling the ASDs in Fig. 2 with a random phase. Although these simulations do not yield strict upper bounds, they also lack the phase information, so that simulations can be interpreted as an additional measure of worst-case performance.

The integrated beam motion (IBM) up to 1 kHz, i.e. the square root of the integral of the PSD, is summarised for all primary BPMs in Table 2. The results show that the upper bound from Eq. (9) yields a conservative estimate that is more than two times larger than the attenuation expected from simulations. However, except for the primary BPMs of the long straight in the vertical direction, the upper bound is below the target deviation, indicating that the Diamond-II specifications are met. For the long straights, the IBM is up to 0.04 µm above target for the upper bound, but below target in simulations. Since the PSD lacks phase information, the Diamond-II disturbance does not reflect the characteristic modal distribution caused by input disturbances and the regularisation significantly impacts the controller performance. However, given that most of the Diamond-II disturbances are input disturbances, it can be expected that the targets will also be met on the long straights.

TESTS ON THE EXISTING DIAMOND STORAGE RING

As part of the FOFB design for Diamond-II, the GSVD-based controller has been implemented and tested on the existing Diamond storage ring. The aim of these experiments is to evaluate the controller in practice, i.e. investigate the FOFB with $n_f < n_s$ and model uncertainty, and to test new FOFB configurations, such as the centralised topology used at Diamond-II. The control system is implemented on a VadaTech AMC540 – a board combining a Xilinx Virtex-7 FPGA with two Texas Instruments (TI) DSPs [17] – and interfaced with the FOFB communication network. The existing 24 computing nodes from all the cells in the storage ring are bypassed, and the communication network reconfigured to form the centralised topology used at Diamond-II. The FPGA on the AMC540 is used for signal routing, and the DSPs are used to produce the corrector inputs for the horizontal and vertical directions. During tests with the AMC540, the time delay is increased from 700 µs to 900 µs and the communication network additionally broadcasts setpoints for the correctors.

As the FOFB at Diamond uses only one corrector type, a subset of $n_u = 160$ correctors and $n_y = 96$ BPMs is selected

ISBN: 978-3-95450-236-3 ISSN: 2673-5350 doi:10.18429/JACoW-IBIC2023-MO2I02

Table 2: Targets and expected IBMs up to 1 kHz for Diamond-II at upstream (US) and downstream (DS) primary BPMs on long straights (LS), mid straights (MS), and standard straights (SS). All values are in µm. The disturbance corresponds to FOFB disabled, and the bound is obtained from Eq. (9).

	Horizontal						Vertical					
	LS US	**LS DS**	**MS US**	**MS DS**	**SS US**	**SS DS**	**LS US**	**LS DS**	**MS US**	**MS DS**	**SS US**	**SS DS**
Disturbance	0.64	0.72	0.45	0.48	0.6	0.61	0.25	0.25	0.21	0.2	0.22	0.21
Target	1.20	1.20	0.90	0.90	0.97	0.97	0.23	0.23	0.14	0.14	0.18	0.18
Bound	0.53	0.41	0.21	0.25	0.2	0.48	0.24	0.27	0.11	0.07	0.13	0.11
Simulation	0.16	0.18	0.06	0.07	0.04	0.11	0.15	0.20	0.07	0.03	0.07	0.06

and represented as in Eq. (2) with $g_s(s) = g_f(s) = g(s)$ and $\tau_d = 900\,\mu s$. The correctors are divided into $n_s = 96$ "slow" and $n_f = 64$ "fast" correctors, and the controller is designed using the GSVD-based approach with $\omega_{tiso} = 2\pi \times 176\,rad\,s^{-1}$ and $\omega_{siso} = 2\pi \times 50\,rad\,s^{-1}$. With this choice of parameters, the sensitivity overshoot is 3.4 dB at 300 Hz.

The GSVD-based controller is compared with a "standard" IMC controller that controls the same $n_y = 96$ BPMs and $n_s = 96$ correctors, but with all n_u correctors tuned to a closed-loop bandwidth of $2\pi \times 176\,rad\,s^{-1}$. All algorithms are evaluated on the storage ring at 300 mA beam current and with wigglers disabled.

The horizontal IBMs measured at BPM 1 are compared in Fig. 4, which also shows the disturbance recorded before the experiments (with FOFB disabled) and the corresponding simulated attenuation. As expected from the lower SISO bandwidths, the GSVD-based controller performs worse than the standard controller, but the results show that both controllers yield similar closed-loop bandwidths. The performance differences between standard and GSVD-based controllers are within 0.01 µm for frequencies below 10 Hz, and decrease for higher frequencies, which is in line with theoretical expectations. Comparing the simulation with the real-world results, the simulations perform slightly worse in the horizontal plane, but better in the vertical plane. The differences could be caused by various factors, including model uncertainty or time varying disturbance spectra.

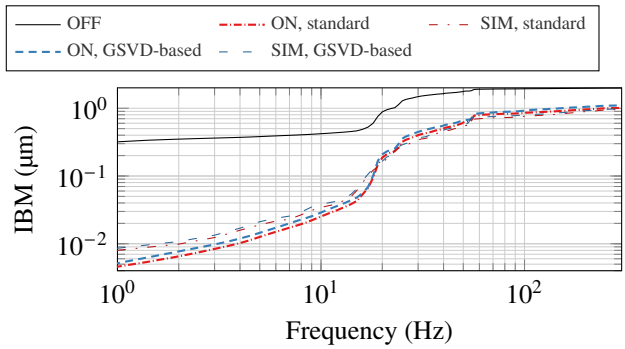

Figure 4: Measured (OFF, ON) and simulated (SIM) horizontal IBM for BPM 1 of the Diamond storage ring with FOFB disabled, standard and GSVD-based IMC.

CONCLUSION

In this paper we have proposed a joint control method for the FOFB at Diamond-II that will use slow and fast correctors. The performance of our method was evaluated using PSD estimates of the disturbance at Diamond-II. We calculated a worst-case upper bound that meets the performance criteria except for the primary BPMs in the long straight that exceed the target by 0.002 µm (0.9 %) in the vertical plane. However, simulations using sampled disturbance show that this upper bound may be conservative. Once the fast correctors are prototyped, the actuator dynamics and the latency will be updated, which is likely to result in better performance estimates.

To demonstrate our algorithm in practice, we integrated a new computing node in the existing storage ring and implemented a GSVD-based controller, splitting the control effort onto designated slow and fast correctors. The results from tests on the storage ring showed that although only a subset of the correctors covered the full bandwidth, the performance of the controller with two corrector types was nearly as good as the one with one corrector type, and that the simulations accurately reflect experimental measurements.

Even though the simulation and real-world results proved the feasibility for Diamond-II, several research questions remain. The mid-ranging approach requires inverting $g_s(s)$ and $g_f(s)$, but for Diamond-II the fast correctors may be such that $g_f(0) = 0$. The mid-ranging approach may therefore result in undesirable integrating behaviour for the fast correctors. To avoid this problem, one solution would be to invert only parts of $g_f(s)$ and quantify the resulting performance loss. Alternatively, one could combine the generalised modal decomposition with a $\mathcal{H}_2$ or $\mathcal{H}_\infty$ controller design [15], which may also reduce the sensitivity peaks.

While upper bounds showed that most performance requirements for Diamond-II are met, simulations using sampled Diamond-II data and tests on the existing facility showed that these upper bounds are conservative. To obtain less conservative bounds, future research could extend the disturbance data using phase information, e.g. by aggregating the different disturbance sources and modelling their spatial impact onto the storage ring.

ISBN: 978-3-95450-236-3 ISSN: 2673-5350 doi:10.18429/JACoW-IBIC2023-MO2I02

REFERENCES

[1] M. G. Abbott *et al.*, "Diamond-II technical design report," Diamond Light Source, Tech. Rep., Aug. 2022. https://www.diamond.ac.uk/Home/News/LatestNews/2022/14-10-22.html

[2] S. R. Duncan and W. Heath, "The robustness of multi-array cross-directional control systems," in *Proc. Contr. Sys. Conf.*, Stockholm, Sweden, Sep. 2010, pp. 180–185.

[3] S. Gayadeen, S. R. Duncan, and W. P. Heath, "Design of multi-array controllers for electron beam stabilisation on synchrotrons," in *Proc. Amer. Contr. Conf. (ACC'13)*, Washington, DC, USA, Jun. 2013, pp. 1201–1206. doi:10.1109/ACC.2013.6579999

[4] G. H. Golub and C. F. Van Loan, *Matrix Computations*, 4th ed. The Johns Hopkins Univ. Press, 2013.

[5] N. Hubert, L. Cassinari, J. C. Denard, A. Nadji, and L. Nadolski, "Global Fast Orbit Feedback System Down to DC using Fast and Slow Correctors," in *Proc. Eur. Workshop Beam Diagn. Instrum. Part. Accel. (DIPAC'09)*, Basel, Switzerland, May 2009, pp. 27–31. https://jacow.org/d09/papers/MOOC01.pdf

[6] C. Steier, E. Domning, T. Scarvie, and E. Williams, "Operational Experience Integrating Slow and Fast Orbit Feedbacks at the ALS," in *Proc. Eur. Part. Accel. Conf. (EPAC'04)*, Lucerne, Switzerland, Jul. 2004, pp. 2786–2788. http://jacow.org/e04/papers/THPLT141.pdf

[7] E. Plouviez and F. Uberto, "The Orbit Correction Scheme of the New EBS of the ESRF," in *Proc. of Int. Beam Instrum. Conf. (IBIC'16)*, Barcelona, Spain, Sep. 2016, pp. 51–54. doi:10.18429/JACoW-IBIC2016-MOPG09

[8] C. Schwartz and L. Emery, "Compensating the Frequency Deadband of the APS Real-Time and DC Transverse Orbit Correction Systems," in *Proc. Part. Accel. Conf. (PAC'01)*, Chicago, IL, USA, Jun. 2001, pp. 1234–1236. https://jacow.org/p01/papers/TPAH001.pdf

[9] L. H. Yu, S. Krinsky, O. Singh, and F. J. Willeke, "The Performance of a Fast Closed Orbit Feedback System with Combined Fast and Slow Correctors," in *Proc. Eur. Part. Accel. Conf. (EPAC'08)*, Genoa, Italy, Jun. 2008, pp. 3315–3317. https://jacow.org/e08/papers/THPC140.pdf

[10] S. Gayadeen and S. R. Duncan, "Discrete-time anti-windup compensation for synchrotron electron beam controllers with rate constrained actuators," *Automatica*, vol. 67, pp. 224–232, May 2016. doi:10.1016/j.automatica.2016.01.037

[11] E. Plouviez, F. Epaud, F. Farvacque, and J. M. Koch, "Optimisation of the SVD treatment in the fast orbit correction of the ESRF storage ring," in *Proc. Int. Beam Instrum. Conf. (IBIC'13)*, Oxford, UK, Sep. 2013, pp. 694–697. https://jacow.org/IBIC2013/papers/WEPC13.pdf

[12] E. Plouviez, F. Epaud, J. M. Koch, and M. B. Scheidt, "The new fast orbit correction system of the ESRF storage ring," in *Proc. Eur. Workshop Beam Diagn. Instrum. Part. Accel. (DIPAC'11)*, Hamburg, Germany, May 2011, pp. 215–217. https://jacow.org/DIPAC2011/papers/MOPD74.pdf

[13] I. Kempf, P. J. Goulart, and S. Duncan, "Control of Two-Array Cross-Directional Systems using the Generalised Singular Value Decomposition," *arXiv*, 2023. doi:10.48550/arXiv.2308.08631

[14] I. P. S. Martin *et al.*, "Orbit Stability Studies for the Diamond-II Storage Ring," in *Proc. Int. Part. Accel. Conf. (IPAC'22)*, Bangkok, Thailand, Jul. 2022, pp. 2602–2605. doi:10.18429/JACoW-IPAC2022-THPOPT017

[15] M. Morari and E. Zafiriou, *Robust Process Control*, 1st ed. Prentice-Hall, 1989.

[16] B. J. Allison and A. J. Isaksson, "Design and performance of mid-ranging controllers," *J. Proc. Contr.*, vol. 8, no. 5, pp. 469–474, Oct. 1998. doi:10.1016/S0959-1524(98)00012-2

[17] VadaTech, *Xilinx Virtex-7 FPGA AMC with dual TI DSP (AMC540)*, 4FM737-12, 2019.